

ScatterFormer: Efficient Voxel Transformer with Scattered Linear Attention

Chenheng He¹, Ruihuang Li^{1,2}, Guowen Zhang¹, Lei Zhang^{1,2}

¹The Hong Kong Polytechnic University

²OPPO Research Institute

Abstract

Window-based transformers have demonstrated strong ability in large-scale point cloud understanding by capturing context-aware representations with affordable attention computation in a more localized manner. However, because of the sparse nature of point clouds, the number of voxels per window varies significantly. Current methods partition the voxels in each window into multiple subsets of equal size, which cost expensive overhead in sorting and padding the voxels, making them run slower than sparse convolution based methods. In this paper, we present ScatterFormer, which, for the first time to our best knowledge, could directly perform attention on voxel sets with variable length. The key of ScatterFormer lies in the innovative Scatter Linear Attention (SLA) module, which leverages the linear attention mechanism to process in parallel all voxels scattered in different windows. Harnessing the hierarchical computation units of the GPU and matrix blocking algorithm, we reduce the latency of the proposed SLA module to less than 1 ms on moderate GPUs. Besides, we develop a cross-window interaction module to simultaneously enhance the local representation and allow the information flow across windows, eliminating the need for window shifting. Our proposed ScatterFormer demonstrates 73 mAP (L2) on the large-scale Waymo Open Dataset and 70.5 NDS on the NuScenes dataset, running at an outstanding detection rate of 28 FPS. Code is available at <https://github.com/skyhehe123/ScatterFormer>.

1. Introduction

In the field of 3D object detection, the use of point clouds has become increasingly popular, especially for providing accurate and reliable perception results in autonomous systems. Unlike image data, point clouds obtained from LiDAR are often sparse and non-uniformly distributed, with varying density according to their distances from the sensor. Earlier approaches utilize point cloud operators like PointNet++ [29] for feature extraction in continuous space [35]. Some approaches [5, 10, 14, 18, 49, 50, 52, 59] have transformed point clouds into voxel grids, which are then

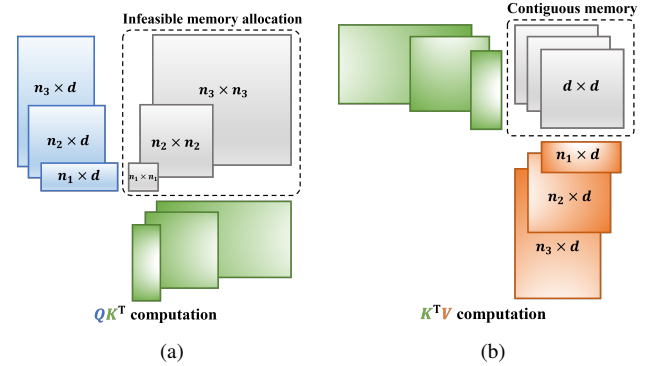


Figure 1. Illustration of (a) traditional attention and (b) our proposed linear attention on variable-length sequences.

efficiently processed by a sparse convolutional neural network (SpCNN) [49].

Recently, the success of vision transformers [7, 21] has motivated a number of attention-based methods for processing indoor point clouds [12, 22, 24, 25, 27, 56]. Inspired by SwinTransformer [21], various studies [9, 15, 23, 47] have advanced the application of window-based Transformers in large-scale 3D detection tasks within outdoor environments, achieving outstanding performance and highlighting their potential as alternatives to SpCNN. However, due to the inherent sparsity of point clouds, the number of features grouped by windows can vary significantly, hampering the parallelism in attention computation. To resolve this issue, SST [9] batches windows based on the number of voxels within them and manages the attention computation in a hybrid serial-parallel manner. VoxSet [15] processes each window through a set of proxy codes. Further advances in [23, 47] partition the voxels within a window into subsets of fixed size by sorting them from different axes. Albeit effective, these methods require extensive sorting and padding operations, incurring substantial memory and computational overhead.

In this paper, we revisit the computation of attention on the voxels grouped by windows and delve into attention computation from the perspective of variable-length matrices. As shown in Figure 1(a), given voxels grouped by windows $\{V_1 \in \mathbb{R}^{n_1 \times d}, V_2 \in \mathbb{R}^{n_2 \times d}, \dots, V_k \in \mathbb{R}^{n_k \times d}\}$, the

attention matrices $\{A_1 \in \mathbb{R}^{n_1 \times n_1}, A_2 \in \mathbb{R}^{n_2 \times n_2}, \dots, A_k \in \mathbb{R}^{n_k \times n_k}\}$ consume quadratic memory and are difficult to assign in a contiguous space. This makes the attention computation on variable-length matrices infeasible, especially when there is a large amount of voxels in some areas.

Recent efforts on linear attention [1, 13, 17, 48] have showcased the potential of using kernel functions on queries and keys to approximate their softmax-based attention matrix, *i.e.*, $\phi(Q) \cdot \phi(K)^T \approx \text{softmax}(QK^T)$. By this means, we can achieve linear complexity by switching the computation order from $(Q \cdot K^T) \cdot V$ to $Q \cdot (K^T \cdot V)$. Building upon this concept, we introduce **Scatter Linear Attention** (SLA), which extends linear attention to accommodate voxel transformer and showcase an ultra-fast and memory-efficient attention on variable-length voxel sets. As shown in Figure 1(b), for each window, we calculate the cross-covariance matrix between K and V . Thus we can maintain an $m \times d \times d$ matrix in contiguous memory, where m denotes the number of nonempty windows and d represents the feature dimension. Specifically, we can flatten the voxels of the entire scene into a single matrix and develop a scattered matrix multiplication operation, where the matrix multiplication are executed in parallel on the sub-matrices of input matrix, generating contextual information of each window. Inspired by FlashAttention [6], we accelerate this operation through a matrix blocking algorithm, where the sub-matrices are further divided into regular blocks and processed using the SRAM units within the GPU. It is found that our implementation is significantly more efficient than using existing tensor computation libraries such as PyTorch, which makes the latency of our model comparable to convolutional based detector [52].

In addition, it is observed that window-based transformer models perform window shifting across stages. This results in substantial permutation operations on voxel features, leading to undesirable computational overhead. To address this issue, we propose a cross-window interaction (CWI) module, which is composed of depth-wise convolutions with small 2D kernels and lengthy 1D kernels that allow the voxel features in each window to fully interact with the features in other windows. As a results, the proposed CWI module can improve both the locality and the long-range dependency of the voxel features while requiring minimal computational effort.

Building upon the SLA and CWI modules, we propose the **ScatterFormer**, an innovative voxel transformer for large-scale point cloud understanding. Our experiments show that ScatterFormer achieves linear complexity without compromising accuracy. It achieves superior results compared to the state-of-the-art model DSVT [47]. The latency of ScatterFormer is significantly lower than that of transformer-based detectors [9, 15, 47], which is comparable to that of the sparse convolution-based detectors [52].

In summary, we delve into attention on voxels grouped by windows, highlighting the challenges in memory allocation and computation for variable-length matrices. Then we introduce an SLA module, which adapts the linear attention mechanism and a specially designed matrix multiplication algorithm to efficiently process voxels grouped by windows. Finally, we present ScatterFormer, which has linear complexity and can efficiently process large-scale LiDAR scenes, achieving competitive accuracy with lower latency compared to existing transformer-based detectors.

2. Related Work

2.1. Point Cloud-based 3D Object Detection

There exist two primary point-cloud representations in 3D object detection, *i.e.*, point-based and voxel-based ones. In point-based methods [30, 31, 35, 39, 54], point clouds are first passed through a point-based backbone network [28], in which the points are gradually sampled and features are learned by point cloud operators. F-Pointnet [30] first employs PoinNet to detect 3D objects based on the frustums lifted by 2D proposals. PointRCNN [35] directly generates 3D proposals from point-based features with foreground segmentation. VoteNet [31] clusters objects from the surface points using a deep Hough voting method. Other point operators based on point graph [39, 54] and range-view [8] have also been developed for point cloud processing.

Point-based methods are primarily limited by their inference efficiency and the absence of contextual features in a continuous space. On the other hand, voxel-based approaches [5, 14, 18, 49, 52, 57, 59] transform the entire point clouds into regular grids through voxelization, showcasing superior efficiency and context representation. VoxelNet [59] proposes a voxel feature encoding (VFE) module and combines it with 3D convolutions to extract voxel features in an end-to-end manner. SECOND [49] optimizes 3D convolution for sparse data, resulting in significant reduction in both time and memory. PointPillars [18] demonstrates an efficient model by stacking voxels into vertical columns, subsequently processing them with naive 2D convolutions. There are also efforts [14, 37] that explore hybrid representations of point-based and voxel-based networks, demonstrating better trade-off between speed and accuracy. However, a common limitation across these methods is their reliance on small convolution kernels with restricted receptive fields, making them less adept at capturing the global context for 3D object detection.

In this paper, we shed light on the voxel-based methods and introduce a novel Scatter Linear Attention module for efficient voxel interactions. By performing linear attention on the voxel features grouped by large windows, we obtain richer context information than those with convolutions.

2.2. Transformer on Point Cloud

Inspired by the significant success of self-attention in NLP [46] and CV [7, 45], Transformers have been adapted for 3D vision due to their ability to capture long-range dependencies. The Point Transformers [27, 56] employ attention to modulate point clouds for classification and segmentation tasks. PCT [12] presents an optimized offset attention module, which, when combined with the implicit Laplacian operator and normal estimation, becomes more adept for point cloud understanding. Some methods like [9, 22] opt for voxels or key-points to optimize latency. 3DETR [25] proposes a query-based 3D object detection scheme. CT3D [33] enhances the region-based network using a channel-wise Transformer framework. To achieve context-rich representations, several studies [9, 15, 23, 24, 47] have integrated the attention module into point- or voxel-based encoders. For instance, VoTr [24] utilizes dilated attention for expanded receptive fields; VoxSet [15] applies set attention for extracting point-based features in set-to-set translation; SST [9] employs local attention with shifted windows; and OcTr [58] adopts an Octree-based attention for efficient hierarchical context learning. Nevertheless, how to efficiently leverage global context from attention remains a challenge due to the intrinsic sparsity of point clouds. DSVT [47] and FlatFormer [23] group the voxels within each window into a series of fixed-length voxel sets, thus extracting the features in a fully parallel manner. However, these approaches more or less lose the spatial proximity and incur extensive computational overhead in grouping the voxels.

3. Method

The overall architecture of our proposed ScatterFormer is depicted in Figure 2. Firstly, we transform the point cloud into a voxel based representation, where each feature corresponds to a token. Following the paradigm in SST [9], we develop a backbone network that is composed by four window-based transformer blocks and perform single-stride feature extraction. Each transformer block incorporates a Scatter Linear Attention (SLA) module for blending tokens within a window, a Cross-window Interaction (CWI) module to ensure information flow across windows, and a Feed-Forward Network (FFN) to enrich the feature representation by mixing their channels. After that, we convert backbone features into a BEV map and apply 2D convolutional neural network to predict bounding-boxes. Our ScatterFormer differs significantly from previous window-based transformer models [9, 23, 47] that require organizing voxel features into fixed-length sets, which allows for more flexible attention computation across windows. Additionally, the CWI module in ScatterFormer eliminates the need for window shifting. These innovative designs enable ScatterFormer to avoid unnecessary memory allocation and permutation op-

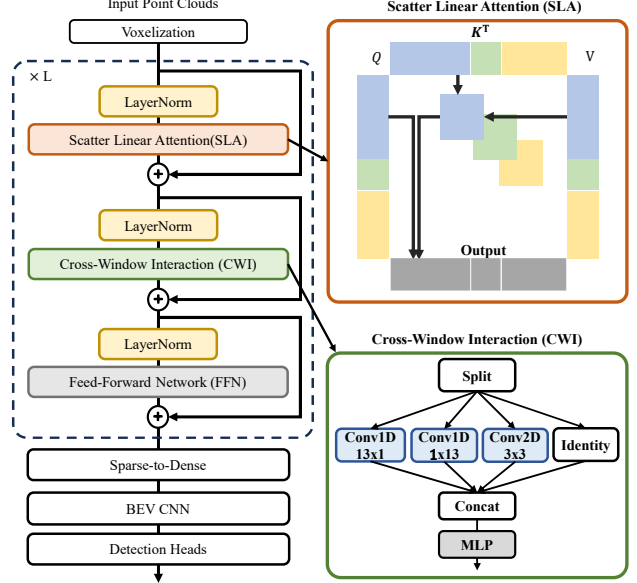


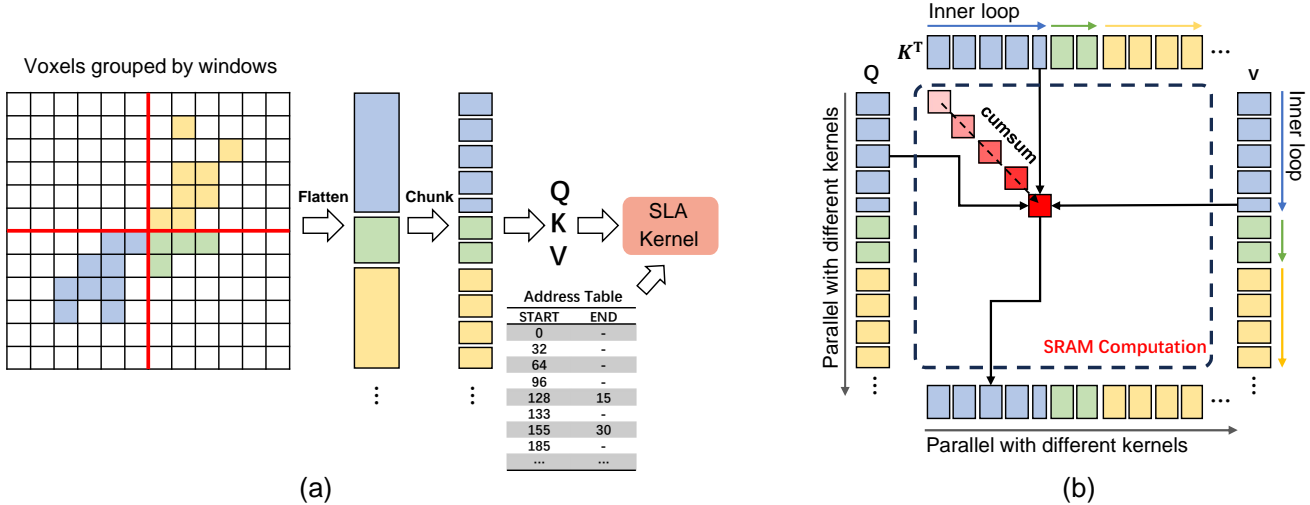
Figure 2. Our ScatterFormer has four encoding stages. Each stage consists of a LayerNorm with a residual connection, a core Scatter Linear Attention (SLA) module, a Cross-Windows Interaction (CWI) module, and a feed-forward network (FFN).

erations, thereby achieving high efficiency comparable to those SpCNN-based models.

3.1. Linear Attention

We begin by revisiting the self-attention as introduced by [46]. Given an input matrix $x \in \mathbb{R}^{N \times d}$, where N denotes the number of tokens and d denotes the dimensionality. Self-attention first linearly projects the input to queries, keys and values using weight matrices W_Q , W_K and W_V , such that $Q = xW_Q$, $K = xW_K$, $V = xW_V$. Then it computes a Softmax-based attention map based on queries and keys, i.e., $A(Q, K) = \text{Softmax}(QK^T)/\sqrt{d}$. The output of the self-attention is defined as the weighted sum of N token features in V with the weights corresponding to the attention map, i.e., $O = A(Q, K)V$. This approach involves calculating the similarity for all query-key pairs, yielding a computational complexity of $O(N^2)$.

Linear attention [1, 17] offers a notable alternative to self-attention by significantly reducing its computational complexity from $O(N^2)$ to $O(N)$. This efficiency is attained through the application of kernel functions on the query (Q) and key (K) matrices, which effectively approximate the original attention map without relying on Softmax, i.e., $A(Q, K) = \phi(Q)\phi(K)^T$. By exploiting the associative property of matrix multiplication, the computation shifts from $(\phi(Q)\phi(K)^T)V$ to $\phi(Q)(\phi(K)^TV)$. This modification leads to a computational complexity proportional to the number of tokens, maintaining an order of $O(N)$.



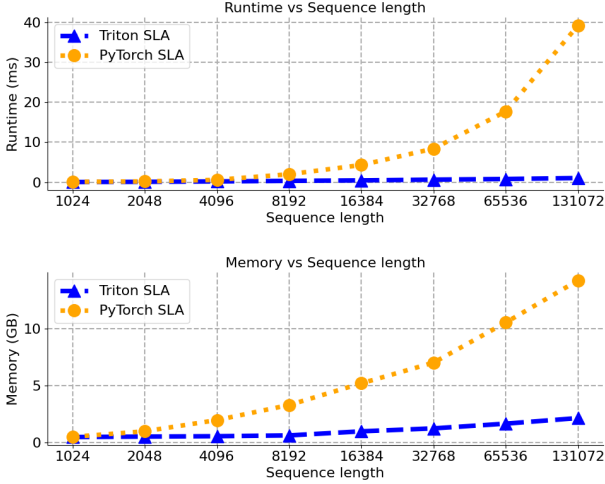


Figure 4. Performance evaluation of SLA implemented by PyTorch (yellow) and Triton (blue).

In our development, we implement the SLA with the Triton [44] GPU programming library, thereby utilizing high-performance tensor cores to achieve block-wise matrix multiplication. As illustrated in Figure 4, our implementation outperforms its PyTorch-based counterpart, demonstrating enhanced speed and reduced memory usage when handling token attention for extremely long sequences.

3.3. Cross Window Interaction

Traditional window-based transformers utilize “Shifted Windows” for inter-window connection. For point cloud sequences, this requires recalculating window coordinates and rearranging matrices. In DSVT, the computation of voxel indices in subsets and the rearrangement of voxel matrices are particularly time-consuming, accounting for 24% of the total backbone latency, as shown in Figure 5. To alleviate this unnecessary computational overhead, we introduce the Cross-Window Interaction (CWI) module, which employs convolutions with kernel size spanning across windows to blend voxel features across windows. This shift-free strategy enables ScatterFormer to achieve higher computational utilization for feature extraction.

Specifically, we follow the Inception [42] to divide the features into different branches. One branch applies a $1 \times (S_h + 1)$ convolution and another applies a $(S_w + 1) \times 1$ convolution, where (S_w, S_h) represents the window size. We also incorporate a regular 3×3 convolution in one branch for local feature enhancement and leave one branch for identity mapping. Given input X of channel $4c$, the output X' of the CWI module can be written as:

$$X' = \text{Concat}(X_k, X_w, X_h, X^{3c:4c}), \quad (4)$$

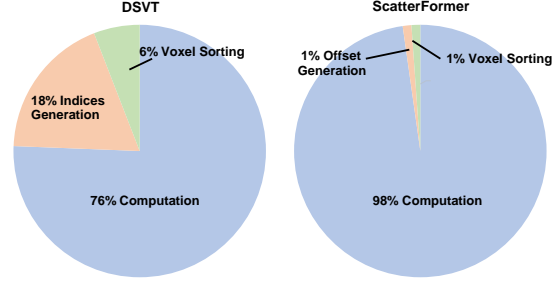


Figure 5. Runtime decomposition of backbone in DSVT [47] and ScatterFormer. The offsets generation represents the access of address table for block-wise matrix computation.

where

$$X_k = \text{DWConv}_{1 \times (S_h + 1)}(X^{:c}), \quad (5)$$

$$X_w = \text{DWConv}_{(S_w + 1) \times 1}(X^{c:2c}), \quad (6)$$

$$X_h = \text{DWConv}_{3 \times 3}(X^{2c:3c}). \quad (7)$$

In our experiments, we found that CWI can help the model to establish long-range dependencies quickly. The cross-window kernels enable each token within a window to blend with tokens from other windows, not only at the boundaries.

Detection Head and Loss. To complement existing detection heads, ScatterFormer generates dense BEV feature maps from sparse voxel representations by assigning them back to their spatial locations and filling the unoccupied positions with zeros. For the BEV network, we simply follow CenterPoint-Pillar [52], adopting a CNN with convolutional layers in two levels of strides. Each layer involves two convolutions for down-sampling and one for up-sampling. The convolutional features from different scales are finally concatenated and passed to the detection head for bounding-box prediction. In terms of the detection head and loss function, we utilize a setup identical to that employed in DSVT [47]. We train the detection model with heatmap estimation, bounding-box regression, and incorporate an IoU loss for confidence calibration. On the nuScenes dataset, we adapt the head architecture from Transfusion [2].

4. Experiments

4.1. Datasets and Evaluation Metrics

Waymo Open Dataset (WOD). This dataset contains 230,000 annotated samples split into 160,000 for training, 40,000 for validation, and 30,000 for testing. It uses two metrics for 3D object detection: mean average precision (mAP) and mAP weighted by heading accuracy (mAPH), further categorized into Level 1 (L1) for objects detected by over five LiDAR points, and Level 2 (L2) for those detected with at least one point.

NuScenes. This dataset comprises 40,000 annotated samples, with 28,000 for training, 6,000 for validation, and

Table 1. Performance comparison on the validation set of Waymo Open Dataset. Symbol ‘*’ denotes the methods with temporal modeling, and ‘-’ means that the result is not available.

Method	Frames	ALL (3D mAPH)		Vehicle (AP/APH)		Pedestrian (AP/APH)		Cyclist (AP/APH)	
		L1	L2	L1	L2	L1	L2	L1	L2
SECOND [49]	1	63.05	57.23	72.27 / 71.69	63.85 / 63.33	68.70 / 58.18	60.72 / 51.31	60.62 / 59.28	58.34 / 57.05
PointPillar [18]	1	63.33	57.53	71.60 / 71.00	63.10 / 62.50	70.60 / 56.70	62.90 / 50.20	64.40 / 62.30	61.90 / 59.90
IA-SSD [55]	1	64.48	58.08	70.53 / 69.67	61.55 / 60.80	69.38 / 58.47	60.30 / 50.73	67.67 / 65.30	64.98 / 62.71
LiDAR R-CNN [20]	1	66.20	60.10	73.50 / 73.00	64.70 / 64.20	71.20 / 58.70	63.10 / 51.70	68.60 / 66.90	66.10 / 64.40
RSN [40]	1	-	-	75.10 / 74.60	66.00 / 65.50	77.80 / 72.70	68.30 / 63.70	-	-
PV-RCNN [37]	1	69.63	63.33	77.51 / 76.89	68.98 / 68.41	75.01 / 65.65	66.04 / 57.61	67.81 / 66.35	65.39 / 63.98
Part-A2 [36]	1	70.25	63.84	77.05 / 76.51	68.47 / 67.97	75.24 / 66.87	66.18 / 58.62	68.60 / 67.36	66.13 / 64.93
Centerpoint [52]	1	-	65.50	-	- / 66.20	-	- / 62.60	-	- / 67.60
VoTR [24]	1	-	-	74.95 / 74.25	65.91 / 65.29	-	-	-	-
VoxSeT [15]	1	72.24	66.22	74.50 / 74.03	65.99 / 65.56	80.03 / 72.42	72.45 / 65.39	71.56 / 70.29	68.95 / 67.73
SST-1f [9]	1	-	-	76.22 / 75.79	68.04 / 67.64	81.39 / 74.05	72.82 / 65.93	-	-
SWFormer-1f [41]	1	-	-	77.8 / 77.3	69.2 / 68.8	80.9 / 72.7	72.5 / 64.9	-	-
PillarNet [34]	1	74.60	68.43	79.09 / 78.59	70.92 / 70.46	80.59 / 74.01	72.28 / 66.17	72.29 / 71.21	69.72 / 68.67
PV-RCNN++ [37]	1	75.21	68.61	79.10 / 78.63	70.34 / 69.91	80.62 / 74.62	71.86 / 66.30	73.49 / 72.38	70.70 / 69.62
FlatFormer [23]	1	-	67.2	- / -	69.0 / 68.6	- / -	71.5 / 65.3	- / -	68.6 / 67.5
PillarNext-1f [19]	1	75.74	69.74	78.40 / 77.90	70.27 / 69.81	82.53 / 77.14	74.90 / 69.80	73.21 / 72.20	70.58 / 69.62
VoxelNext [5]	1	76.3	70.1	78.2 / 77.7	69.9 / 69.4	81.5 / 76.3	73.5 / 68.6	76.1 / 74.9	73.3 / 72.2
FSD [10]	1	77.3	70.8	79.2 / 78.8	70.5 / 70.1	82.6 / 77.3	73.9 / 69.1	77.1 / 76.0	74.4 / 73.3
DSVT-1f [47]	1	78.2	72.1	79.7 / 79.3	71.4 / 71.0	83.7 / 78.9	76.1 / 71.5	77.5 / 76.5	74.6 / 73.7
ScatterFormer-Lite (ours)	1	77.0	70.7	78.2 / 78.5	70.5 / 69.9	82.3 / 77.5	72.4 / 68.8	75.4 / 75.0	74.2 / 73.3
ScatterFormer (ours)	1	79.3	73.6	80.4 / 79.9	72.8 / 72.4	84.1 / 81.1	77.0 / 74.1	77.3 / 76.8	75.2 / 74.3
SST-3f [9]	3	-	-	78.66 / 78.21	69.98 / 69.57	83.81 / 80.14	75.94 / 72.37	-	-
FlatFormer-3f [23]	3	-	72.0	- / -	71.4 / 71.0	- / -	74.5 / 71.3	- / -	74.7 / 73.7
SWFormer-3f [41]	3	-	-	79.4 / 78.9	71.1 / 70.6	82.9 / 79.0	74.8 / 71.1	-	-
PillarNext-3f [19]	3	80.0	74.5	80.6 / 80.1	72.9 / 72.4	85.0 / 82.1	78.0 / 75.2	78.9 / 77.9	76.7 / 75.7
DSVT-4f [47]	4	81.3	75.6	81.8 / 81.4	74.1 / 73.6	85.6 / 82.8	78.6 / 75.9	80.4 / 79.6	78.1 / 77.3
ScatterFormer-Lite-4f (ours)	4	79.1	74.2	79.4 / 79.5	72.3 / 72.5	84.2 / 81.4	77.2 / 75.1	78.2 / 76.5	76.1 / 74.9
ScatterFormer-4f (ours)	4	81.5	76.5	82.7 / 81.9	75.0 / 74.5	86.5 / 83.7	80.2 / 77.5	79.8 / 79.0	78.5 / 77.4
*3D-MAN [51]	16	-	-	74.53 / 74.03	67.61 / 67.14	71.7 / 67.7	62.6 / 59.0	-	-
*CenterFormer [60]	4	77.0	73.2	78.1 / 77.6	73.4 / 72.9	81.7 / 78.6	77.2 / 74.2	75.6 / 74.8	73.4 / 72.6
*CenterFormer [60]	8	77.3	73.7	78.8 / 78.3	74.3 / 73.8	82.1 / 79.3	77.8 / 75.0	75.2 / 74.4	73.2 / 72.3
*MPPNet [4]	4	79.83	74.22	81.54 / 81.06	74.07 / 73.61	84.56 / 81.94	77.20 / 74.67	77.15 / 76.50	75.01 / 74.38
*MPPNet [4]	16	80.40	74.85	82.74 / 82.28	75.41 / 74.96	84.69 / 82.25	77.43 / 75.06	77.28 / 76.66	75.13 / 74.52
*MSF [16]	4	80.20	74.62	81.36 / 80.87	73.81 / 73.35	85.05 / 82.10	77.92 / 75.11	78.40 / 77.61	76.17 / 75.40
*MSF [16]	8	80.65	75.46	82.83 / 82.01	75.76 / 75.31	85.24 / 82.21	78.32 / 75.61	78.52 / 77.74	76.32 / 75.47

6,000 for testing. On this dataset, the model performance is measured by mean average precision (mAP) across multiple distance thresholds (0.5, 1, 2, and 4 meters) and the nuScenes detection score (NDS), which combines mAP with a weighted sum of five additional metrics assessing true positive predictions in translation, scale, orientation, velocity, and attribute accuracy.

4.2. Implementation Details

Our approach is implemented using the open source OpenPCDet [43]. To construct ScatterFormer, we set voxel size as (0.32m, 0.32m, 6m) for Waymo and (0.3m, 0.3m, 8m) for NuScenes. The window size (S_w, S_h) for the two datasets are set to (12, 12) and (24, 24), respectively. We stacked 4 building blocks for the backbone network. In Waymo, we set our attention module to have 6 heads with dimensionality of 192. The ScatterFormer was trained for 36 epochs with a learning rate of 0.004. In NuScenes, we employ 4 heads with a dimensionality of 128. The ScatterFormer was trained for 20 epochs with a learning rate of 0.005. We use

8 RTX A6000 GPUs to train our models with a batch size equal to 32. Other settings for training and inference are strictly adhered to DSVT [47].

We also developed a lighter version of ScatterFormer, termed **ScatterFormer-Lite**, as shown in Figure 6. It is composed of four stages with a reduced feature dimensionality of 128. The input voxel of ScatterFormer-Lite has a size of (0.08m, 0.08m, 6m). The first two stages involve a residual convolutional module to learn local features, which can be defined as:

$$\hat{x} = \text{ReLU}(\text{BN}(\text{SpConv3x3}(x))), \quad (8)$$

$$x = \text{BN}(\text{SpConv3x3}(\hat{x})) + x. \quad (9)$$

The voxel features are further down-sampled through a sub-manifold max-pooling layer. The final two stages incorporate the core feature encoding blocks that are used in the ScatterFormer backbone network.

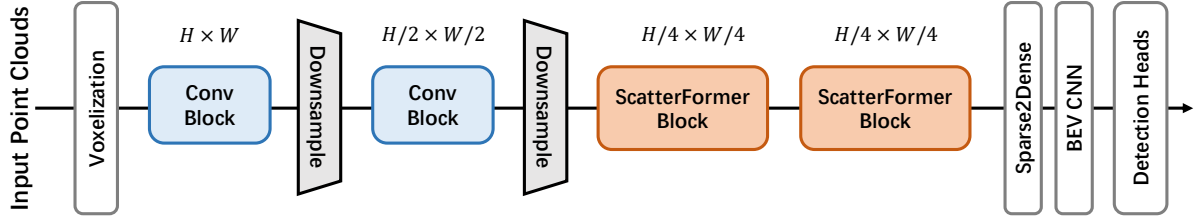


Figure 6. The network architecture of ScatterFormer-Lite.

Table 2. Performance comparison on the test set of Waymo Open Dataset. ‘-’ means that the result is not available.

Method	ALL (3D mAPH)		Vehicle (AP / APH)		Pedestrian (AP / APH)		Cyclist (AP / APH)	
	L1	L2	L1	L2	L1	L2	L1	L2
PointPillar[18]	-	-	68.10	60.10	68.00 / 55.50	61.40 / 50.10	-	-
StarNet[26]	-	-	61.00	54.50	67.80 / 59.90	61.10 / 54.00	-	-
M3DETR[11]	67.1	61.9	77.7 / 77.1	70.5 / 70.0	68.2 / 58.5	60.6 / 52.0	67.3 / 65.7	65.3 / 63.8
3D-MAN [51]	-	-	78.28	69.98	69.97 / 65.98	63.98 / 60.26	-	-
PV-RCNN++ [38]	75.7	70.2	81.6 / 81.2	73.9 / 73.5	80.4 / 75.0	74.1 / 69.0	71.9 / 70.8	69.3 / 68.2
CenterPoint [52]	77.2	71.9	81.1 / 80.6	73.4 / 73.0	80.5 / 77.3	74.6 / 71.5	74.6 / 73.7	72.2 / 71.3
RSN [40]	-	-	80.30	71.60	78.90 / 75.60	70.70 / 67.80	-	-
SST-3f [9]	78.3	72.8	81.0 / 80.6	73.1 / 72.7	83.3 / 79.7	76.9 / 73.5	75.7 / 74.6	73.2 / 72.2
HEDNet [53]	79.05	73.77	83.78 / 83.39	76.33 / 75.96	83.46 / 78.98	77.53 / 73.25	75.86 / 74.78	73.13 / 72.09
PillarNext-3f [19]	79.00	74.09	83.28 / 82.83	76.18 / 75.76	84.40 / 81.44	78.84 / 75.98	73.77 / 72.73	71.56 / 70.55
ScatterFormer-4f (ours)	80.71	75.91	85.45 / 85.04	78.54 / 78.15	84.48 / 81.56	79.06 / 76.25	76.42 / 75.55	74.16 / 73.31

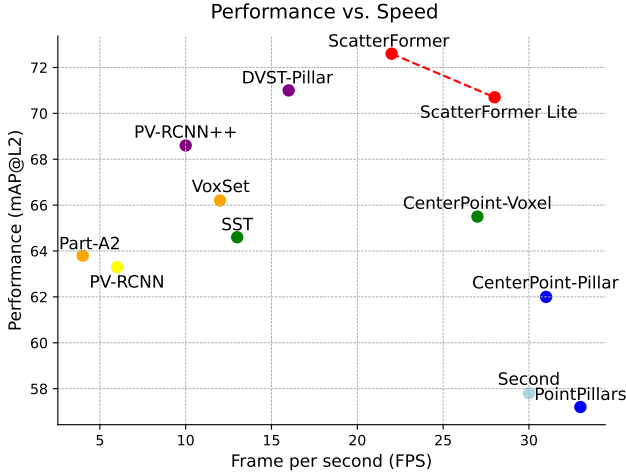


Figure 7. The detection performance (mAPH/L2) vs. speed (FPS) of different methods on Waymo validation set. The speeds of all methods are measured on an NVIDIA A100 GPU.

4.3. Comparison with State-of-the-Arts

Results on Waymo Open Dataset (WOD). We compare ScatterFormer with the published results on the validation set of WOD. As a common practice, we list the methods using single-frame and multi-frame approaches separately. For completeness, we also compare with methods that involve long-term temporal modeling [4, 16, 60]. As demonstrated in Table 1, our single-stage model outperforms most two-stage methods and achieves better perfor-

mance than the state-of-the-art method DSVT [47]. Meanwhile, from Figure 7, it can be seen that our method exhibits a significant improvement in the detection runtime compared to DSVT. This is because our method is based on Linear Attention and it does not require extensive windowing operations. Our lightweight model, ScatterFormer-Lite, also demonstrates overwhelming performance compared to other efficient detection models such as Centerpoint[52] and SECOND [49]. As shown in Table 2, on the Waymo test set, ScatterFormer achieves the highest Level 1 and Level 2 mAPH scores for all categories, underlining its superior detection quality and precision. It is also worth noting that our approach, as a one-shot method, achieves comparable performance to methods that require temporal modeling. This clearly validates the importance of network design in terms of fundamental architecture.

Results on NuScenes. We compare ScatterFormer with the previous best performing methods on the nuScenes dataset. As shown in Table 3, ScatterFormer achieves the on-par performance with the DSVT in terms of NDS (70.5) and the highest mAP of 66.9% among all the competitors. Compared to TransFusion-L [2] which shares the same head as ours, ScatterFormer demonstrates a significant improvements, with 1.4% improvement in mAP, indicating the effective design of its backbone network. ScatterFormer demonstrates especially good performance on small objects, such as motorcycle, bike, traffic lights, indicating that it can effectively encode long-range dependencies.

Table 3. The performance on the validation set of NuScenes.

Method	NDS	mAP	Car	Truck	Bus	T.L.	C.V.	Ped.	M.T.	Bike	T.C.	B.R.
CenterPoint[52]	66.5	59.2	84.9	57.4	70.7	38.1	16.9	85.1	59.0	42.0	69.8	68.3
VoxelNeXt[5]	66.7	60.5	83.9	55.5	70.5	38.1	21.1	84.6	62.8	50.0	69.4	69.4
TransFusion-L[2]	70.1	65.5	86.9	60.8	73.1	43.4	25.2	87.5	72.9	57.3	77.2	70.3
PillarNext[19]	68.4	62.2	85.0	57.4	67.6	35.6	20.6	86.8	68.6	53.1	77.3	69.7
DSVT[47]	71.1	66.4	87.4	62.6	75.9	42.1	25.3	88.2	74.8	58.7	77.8	70.9
ScatterFormer (ours)	70.5	66.9	87.1	60.4	77.8	48.7	28.9	87.7	76.2	59.8	76.1	66.5

Table 4. Ablation experiments on the validation set of Waymo Open Dataset. “SLA” and “CWI” refer to the proposed Scatter Linear Attention and Cross-Window Interaction modules, respectively. “PE” refers to positional embedding. AP and APH scores on LEVEL2 are reported.

	Ablation	Veh.	Ped.	Cyc.
-	baseline	68.3 / 67.9	74.2 / 68.0	71.2 / 70.1
(a)	w/o SLA module	66.1 / 65.1	71.8 / 65.5	67.4 / 66.7
(b)	w/o CWI module	67.2 / 67.1	72.4 / 66.3	69.5 / 68.6
(c)	w/ Shifted-window	67.6 / 67.2	73.0 / 66.9	70.1 / 69.1
(d)	w/o PE	68.0 / 67.5	73.4 / 67.3	70.9 / 69.9

Table 5. Comparison of model performance using different window sizes at various stages. The APH (L2) scores on different categories are reported.

Window Size	#param.	Veh.	Ped.	Cyc.
(12, 12, 12, 12)	7.4M	67.9	68.0	70.1
(12, 12, 24, 24)	7.5M	67.9	68.1	70.5
(24, 24, 24, 24)	7.6M	67.7	67.2	69.4

4.4. Ablation Study

In this section, we conduct ablation experiments on ScatterFormer using 20% of the Waymo training and validation data. Each model was trained for 24 epochs and running on default parameters. Table 4 shows four different configurations of ScatterFormer: (a) removing the Scatter Linear Attention module, (b) removing the CWI module, (c) replacing CWI with Shifted Window, and (d) removing PE.

As can be seen from Table 4, under configuration (a), ScatterFormer performs worse than the baseline by (2.8%, 2.5%, and 3.4%) APH in the three categories. This demonstrates the importance of SLA in capturing long-range contexts and dynamic feature extraction for object detection. In (b), we observe that ScatterFormer, which has lost the ability for cross-window interaction, experiences a performance drop with (0.8%, 1.7%, and 1.5%) APH in the three categories. The Shifted Window paradigm in (c) leads to some improvement but not significant compared to the proposed CWI module. Results in (e) show that PE has a certain effect on performance improvement.

Window Size. In Table 5, we compare the performance

Table 6. Performance with various kernel configurations in the Cross-Window Integration (CWI) module. Each configuration is specified by the notation “KxDy”, where “Kx” refers to the kernel size, and “Dy” denotes the dilation rate. The APH (L2) scores on different categories are reported.

Kernel	Latency	Veh.	Ped.	Cyc.
Conv1D _{K13} × 2	45ms	67.9	68.0	70.1
Conv2D _{K5D1}	44ms	66.7	67.2	68.4
Conv2D _{K7D1}	52ms	67.5	67.7	70.1
Conv2D _{K13}	66ms	68.1	67.4	70.5

Table 7. Performance with different linear attention designs. The APH (L2) scores on different categories are reported.

Linear Attention	Veh.	Ped.	Cyc.
Efficient Attn [3]	66.3	67.2	68.5
Gated Linear Attn [32]	67.9	68.0	70.2
Focused Linear Attn [13]	67.8	68.2	70.4
XCiT [1]	67.9	68.0	70.1

of our model with different window sizes across various stages. We also adjust the kernel size of the 1D convolution in the CWI module to meet the requirement of connecting windows. The consistency in performance metrics, despite the changes in window size, suggests that the window size is not a critical factor for the model’s effectiveness. This could imply that our model is able to capture the necessary contextual information because the CWI module can effectively integrate contextual information beyond the immediate window, enhancing the model’s ability to make informative predictions.

Cross-Window Kernel. Table 6 presents the performance measures under various kernel configurations in the Cross-Window Interaction (CWI) module. The results imply that a kernel cross the window stride is critical for capturing extended spatial contexts within a given window size. For example, Conv2D_{K7D1} works much better than Conv2D_{K5D1}. However, there is a limit to the benefits by simply increasing the kernel size. For example, with Conv2D_{K13}, the additional computational burden outweighs the slight performance gain. Dilated kernel Conv2D_{K7D1} can increase the receptive field, but it may not surpass the

ability of our axis-decomposed larger kernels.

4.5. Comparison with Different Linear Attention

We also perform experiments on several other linear attentions, including Gated Linear Attention [32], Efficient Attention [3], and Focused Linear Attention [13]. From Table 7, we found that the window-based attention framework is not very sensitive to the form of linear attention, with Efficient Attention performing slightly worse than XcIT [1], while Focused Linear Attention and Gated Linear Attention introduce additional time overhead and learnable parameters, respectively.

5. Conclusion

We presented ScatterFormer, a novel architecture for 3D object detection using point clouds, addressing the challenges associated with processing sparse and unevenly distributed data from LiDAR sensors. Our key contribution lay in the Scatter Linear Attention (SLA) module, which effectively overcame the limitations of traditional attention mechanisms in dealing with voxel features with variable length. SLA combined linear attention with a specially designed matrix multiplication operator, catering to the unique demands of processing voxels grouped by windows. By incorporating SLA and a novel cross-window interaction unit, ScatterFormer delivered high accuracy and low latency, outperforming traditional transformer-based and sparse CNN based detectors in large-scale 3D detection tasks.

References

- [1] Alaaeldin Ali, Hugo Touvron, Mathilde Caron, Piotr Bojanowski, Matthijs Douze, Armand Joulin, Ivan Laptev, Natalia Neverova, Gabriel Synnaeve, Jakob Verbeek, et al. Xcit: Cross-covariance image transformers. *Advances in neural information processing systems*, 34:20014–20027, 2021. 2, 3, 4, 8, 9
- [2] Xuyang Bai, Zeyu Hu, Xinge Zhu, Qingqiu Huang, Yilun Chen, Hongbo Fu, and Chiew-Lan Tai. Transfusion: Robust lidar-camera fusion for 3d object detection with transformers. In *Proceedings of the IEEE/CVF conference on computer vision and pattern recognition*, pages 1090–1099, 2022. 5, 7, 8
- [3] Han Cai, Chuang Gan, and Song Han. Efficientvit: Enhanced linear attention for high-resolution low-computation visual recognition. In *Proceedings of the IEEE/CVF International Conference on Computer Vision*, 2023. 8, 9
- [4] Xuesong Chen, Shaoshuai Shi, Benjin Zhu, Ka Chun Chung, Hang Xu, and Hongsheng Li. Mppnet: Multi-frame feature intertwining with proxy points for 3d temporal object detection. In *European Conference on Computer Vision*, pages 680–697. Springer, 2022. 6, 7
- [5] Yukang Chen, Jianhui Liu, Xiangyu Zhang, Xiaojuan Qi, and Jiaya Jia. Voxelnex: Fully sparse voxelnet for 3d object detection and tracking. In *Proceedings of the IEEE/CVF Conference on Computer Vision and Pattern Recognition*, pages 21674–21683, 2023. 1, 2, 6, 8
- [6] Tri Dao, Daniel Y. Fu, Stefano Ermon, Atri Rudra, and Christopher Ré. FlashAttention: Fast and memory-efficient exact attention with IO-awareness. In *Advances in Neural Information Processing Systems*, 2022. 2, 4
- [7] Alexey Dosovitskiy, Lucas Beyer, Alexander Kolesnikov, Dirk Weissenborn, Xiaohua Zhai, Thomas Unterthiner, Mostafa Dehghani, Matthias Minderer, Georg Heigold, Sylvain Gelly, Jakob Uszkoreit, and Neil Houlsby. An image is worth 16x16 words: Transformers for image recognition at scale. *ICLR*, 2021. 1, 3
- [8] Lue Fan, Xuan Xiong, Feng Wang, Naiyan Wang, and ZhaoXiang Zhang. Rangedet: In defense of range view for lidar-based 3d object detection. In *Proceedings of the IEEE/CVF International Conference on Computer Vision (ICCV)*, pages 2918–2927, 2021. 2
- [9] Lue Fan, Ziqi Pang, Tianyuan Zhang, Yu-Xiong Wang, Hang Zhao, Feng Wang, Naiyan Wang, and Zhaoxiang Zhang. Embracing single stride 3d object detector with sparse transformer. In *Proceedings of the IEEE/CVF conference on computer vision and pattern recognition*, pages 8458–8468, 2022. 1, 2, 3, 6, 7
- [10] Lue Fan, Feng Wang, Naiyan Wang, and Zhaoxiang Zhang. Fully sparse 3d object detection. *Advances in Neural Information Processing Systems*, 35:351–363, 2022. 1, 6
- [11] Tianrui Guan, Jun Wang, Shiyi Lan, Rohan Chandra, Zuxuan Wu, Larry Davis, and Dinesh Manocha. M3detr: Multi-representation, multi-scale, mutual-relation 3d object detection with transformers. In *Proceedings of the IEEE/CVF winter conference on applications of computer vision*, pages 772–782, 2022. 7
- [12] Meng-Hao Guo, Jun-Xiong Cai, Zheng-Ning Liu, Tai-Jiang Mu, Ralph R. Martin, and Shi-Min Hu. Pct: Point cloud transformer. *Computational Visual Media*, 7(2):187–199, 2021. 1, 3
- [13] Dongchen Han, Xuran Pan, Yizeng Han, Shiji Song, and Gao Huang. Flatten transformer: Vision transformer using focused linear attention. In *Proceedings of the IEEE/CVF International Conference on Computer Vision*, pages 5961–5971, 2023. 2, 8, 9
- [14] Chenhang He, Hui Zeng, Jianqiang Huang, Xian-Sheng Hua, and Lei Zhang. Structure aware single-stage 3d object detection from point cloud. In *Proceedings of the IEEE/CVF Conference on Computer Vision and Pattern Recognition*, pages 11873–11882, 2020. 1, 2
- [15] Chenhang He, Ruihuang Li, Shuai Li, and Lei Zhang. Voxel set transformer: A set-to-set approach to 3d object detection from point clouds. In *Proceedings of the IEEE/CVF Conference on Computer Vision and Pattern Recognition*, pages 8417–8427, 2022. 1, 2, 3, 6
- [16] Chenhang He, Ruihuang Li, Yabin Zhang, Shuai Li, and Lei Zhang. Msf: Motion-guided sequential fusion for efficient 3d object detection from point cloud sequences. In *Proceedings of the IEEE/CVF Conference on Computer Vision and Pattern Recognition*, pages 5196–5205, 2023. 6, 7
- [17] Angelos Katharopoulos, Apoorv Vyas, Nikolaos Pappas, and François Fleuret. Transformers are rnns: Fast autoregressive

- transformers with linear attention. In *International conference on machine learning*, pages 5156–5165. PMLR, 2020. 2, 3
- [18] Alex H Lang, Sourabh Vora, Holger Caesar, Lubing Zhou, Jiong Yang, and Oscar Beijbom. Pointpillars: Fast encoders for object detection from point clouds. In *Proceedings of the IEEE Conference on Computer Vision and Pattern Recognition*, pages 12697–12705, 2019. 1, 2, 6, 7
- [19] Jinyu Li, Chenxu Luo, and Xiaodong Yang. Pillarnet: Rethinking network designs for 3d object detection in lidar point clouds. In *Proceedings of the IEEE/CVF Conference on Computer Vision and Pattern Recognition*, pages 17567–17576, 2023. 6, 7, 8
- [20] Zhichao Li, Feng Wang, and Naiyan Wang. Lidar r-cnn: An efficient and universal 3d object detector. In *Proceedings of the IEEE/CVF Conference on Computer Vision and Pattern Recognition (CVPR)*, 2021. 6
- [21] Ze Liu, Yutong Lin, Yue Cao, Han Hu, Yixuan Wei, Zheng Zhang, Stephen Lin, and Baining Guo. Swin transformer: Hierarchical vision transformer using shifted windows. In *Proceedings of the IEEE/CVF International Conference on Computer Vision (ICCV)*, pages 10012–10022, 2021. 1
- [22] Ze Liu, Zheng Zhang, Yue Cao, Han Hu, and Xin Tong. Group-free 3d object detection via transformers. In *Proceedings of the IEEE/CVF International Conference on Computer Vision (ICCV)*, pages 2949–2958, 2021. 1, 3
- [23] Zhijian Liu, Xinyu Yang, Haotian Tang, Shang Yang, and Song Han. FlatFormer: Flattened window attention for efficient point cloud transformer. In *Proceedings of the IEEE/CVF Conference on Computer Vision and Pattern Recognition*, pages 1200–1211, 2023. 1, 3, 6
- [24] Jiageng Mao, Yujing Xue, Minzhe Niu, Haoyue Bai, Jiashi Feng, Xiaodan Liang, Hang Xu, and Chunjing Xu. Voxel transformer for 3d object detection. In *Proceedings of the IEEE/CVF International Conference on Computer Vision (ICCV)*, pages 3164–3173, 2021. 1, 3, 6
- [25] Ishan Misra, Rohit Girdhar, and Armand Joulin. An end-to-end transformer model for 3d object detection. In *Proceedings of the IEEE/CVF International Conference on Computer Vision (ICCV)*, pages 2906–2917, 2021. 1, 3
- [26] Jiquan Ngiam, Benjamin Caine, Wei Han, Brandon Yang, Yuning Chai, Pei Sun, Yin Zhou, Xi Yi, Ouais Al-sharif, Patrick Nguyen, et al. Starnet: Targeted computation for object detection in point clouds. *arXiv preprint arXiv:1908.11069*, 2019. 7
- [27] Xuran Pan, Zhuofan Xia, Shiji Song, Li Erran Li, and Gao Huang. 3d object detection with pointformer. In *Proceedings of the IEEE/CVF Conference on Computer Vision and Pattern Recognition (CVPR)*, pages 7463–7472, 2021. 1, 3
- [28] Charles R Qi, Hao Su, Kaichun Mo, and Leonidas J Guibas. Pointnet: Deep learning on point sets for 3d classification and segmentation. In *Proceedings of the IEEE Conference on Computer Vision and Pattern Recognition*, pages 652–660, 2017. 2
- [29] Charles Ruizhongtai Qi, Li Yi, Hao Su, and Leonidas J Guibas. Pointnet++: Deep hierarchical feature learning on point sets in a metric space. In *Advances in neural information processing systems*, pages 5099–5108, 2017. 1
- [30] Charles R Qi, Wei Liu, Chenxia Wu, Hao Su, and Leonidas J Guibas. Frustum pointnets for 3d object detection from rgb-d data. In *Proceedings of the IEEE Conference on Computer Vision and Pattern Recognition*, pages 918–927, 2018. 2
- [31] Charles R. Qi, Or Litany, Kaiming He, and Leonidas J. Guibas. Deep hough voting for 3d object detection in point clouds. In *Proceedings of the IEEE/CVF International Conference on Computer Vision (ICCV)*, 2019. 2
- [32] Zhen Qin, Dong Li, Weigao Sun, Weixuan Sun, Xuyang Shen, Xiaodong Han, Yunshen Wei, Baohong Lv, Fei Yuan, Xiao Luo, Yu Qiao, and Yiran Zhong. Scaling transormer to 175 billion parameters, 2023. 8, 9
- [33] Hualian Sheng, Sijia Cai, Yuan Liu, Bing Deng, Jianqiang Huang, Xian-Sheng Hua, and Min-Jian Zhao. Improving 3d object detection with channel-wise transformer. In *Proceedings of the IEEE/CVF International Conference on Computer Vision (ICCV)*, pages 2743–2752, 2021. 3
- [34] Guangsheng Shi, Ruifeng Li, and Chao Ma. Pillarnet: Real-time and high-performance pillar-based 3d object detection. In *European Conference on Computer Vision*, pages 35–52. Springer, 2022. 6
- [35] Shaoshuai Shi, Xiaogang Wang, and Hongsheng Li. Point-rcnn: 3d object proposal generation and detection from point cloud. In *Proceedings of the IEEE Conference on Computer Vision and Pattern Recognition*, pages 770–779, 2019. 1, 2
- [36] Shaoshuai Shi, Zhe Wang, Xiaogang Wang, and Hongsheng Li. Part-a² net: 3d part-aware and aggregation neural network for object detection from point cloud. *arXiv preprint arXiv:1907.03670*, 2019. 6
- [37] Shaoshuai Shi, Chaoxu Guo, Li Jiang, Zhe Wang, Jianping Shi, Xiaogang Wang, and Hongsheng Li. Pv-rcnn: Point-voxel feature set abstraction for 3d object detection. In *IEEE/CVF Conference on Computer Vision and Pattern Recognition (CVPR)*, 2020. 2, 6
- [38] Shaoshuai Shi, Li Jiang, Jiajun Deng, Zhe Wang, Chaoxu Guo, Jianping Shi, Xiaogang Wang, and Hongsheng Li. Pv-rcnn++: Point-voxel feature set abstraction with local vector representation for 3d object detection. *International Journal of Computer Vision*, 131(2):531–551, 2023. 7
- [39] Weijing Shi and Raj Rajkumar. Point-gnn: Graph neural network for 3d object detection in a point cloud. In *Proceedings of the IEEE/CVF conference on computer vision and pattern recognition*, pages 1711–1719, 2020. 2
- [40] Pei Sun, Weiyue Wang, Yuning Chai, Gamaleldin El-sayed, Alex Bewley, Xiao Zhang, Cristian Sminchisescu, and Dragomir Anguelov. Rsn: Range sparse net for efficient, accurate lidar 3d object detection. In *Proceedings of the IEEE/CVF Conference on Computer Vision and Pattern Recognition*, pages 5725–5734, 2021. 6, 7
- [41] Pei Sun, Mingxing Tan, Weiyue Wang, Chenxi Liu, Fei Xia, Zhaoqi Leng, and Dragomir Anguelov. Swformer: Sparse window transformer for 3d object detection in point clouds. In *European Conference on Computer Vision*, pages 426–442. Springer, 2022. 6
- [42] Christian Szegedy, Vincent Vanhoucke, Sergey Ioffe, Jon Shlens, and Zbigniew Wojna. Rethinking the inception architecture for computer vision. In *Proceedings of the IEEE con-*

- ference on computer vision and pattern recognition, pages 2818–2826, 2016. 5
- [43] OpenPCDet Development Team. Openpcdet: An open-source toolbox for 3d object detection from point clouds. <https://github.com/open-mmlab/OpenPCDet>, 2020. 6
- [44] Philippe Tillet, H. T. Kung, and David Cox. Triton: An intermediate language and compiler for tiled neural network computations. In *Proceedings of the 3rd ACM SIGPLAN International Workshop on Machine Learning and Programming Languages*, page 10–19, New York, NY, USA, 2019. Association for Computing Machinery. 5
- [45] Hugo Touvron, Matthieu Cord, Matthijs Douze, Francisco Massa, Alexandre Sablayrolles, and Herve Jegou. Training data-efficient image transformers & distillation through attention. In *International Conference on Machine Learning*, pages 10347–10357, 2021. 3
- [46] Ashish Vaswani, Noam Shazeer, Niki Parmar, Jakob Uszkoreit, Llion Jones, Aidan N Gomez, Łukasz Kaiser, and Illia Polosukhin. Attention is all you need. In *Advances in neural information processing systems*, pages 5998–6008, 2017. 3
- [47] Haiyang Wang, Chen Shi, Shaoshuai Shi, Meng Lei, Sen Wang, Di He, Bernt Schiele, and Liwei Wang. Dsvt: Dynamic sparse voxel transformer with rotated sets. In *Proceedings of the IEEE/CVF Conference on Computer Vision and Pattern Recognition*, pages 13520–13529, 2023. 1, 2, 3, 5, 6, 7, 8
- [48] Sinong Wang, Belinda Z. Li, Madian Khabsa, Han Fang, and Hao Ma. Linformer: Self-attention with linear complexity, 2020. 2
- [49] Yan Yan, Yuxing Mao, and Bo Li. Second: Sparsely embedded convolutional detection. *Sensors*, 18(10):3337, 2018. 1, 2, 6, 7
- [50] Bin Yang, Wenjie Luo, and Raquel Urtasun. Pixor: Real-time 3d object detection from point clouds. In *Proceedings of the IEEE Conference on Computer Vision and Pattern Recognition*, pages 7652–7660, 2018. 1
- [51] Zetong Yang, Yin Zhou, Zhifeng Chen, and Jiquan Ngiam. 3d-man: 3d multi-frame attention network for object detection. In *Proceedings of the IEEE/CVF conference on computer vision and pattern recognition*, pages 1863–1872, 2021. 6, 7
- [52] Tianwei Yin, Xingyi Zhou, and Philipp Krahenbuhl. Center-based 3d object detection and tracking. In *Proceedings of the IEEE/CVF conference on computer vision and pattern recognition*, pages 11784–11793, 2021. 1, 2, 5, 6, 7, 8
- [53] Gang Zhang, Junnan Chen, Guohuan Gao, Jianmin Li, and Xiaolin Hu. Hednet: A hierarchical encoder-decoder network for 3d object detection in point clouds. *arXiv preprint arXiv:2310.20234*, 2023. 7
- [54] Yanan Zhang, Di Huang, and Yunhong Wang. Pc-rgnn: Point cloud completion and graph neural network for 3d object detection. In *Proceedings of the AAAI conference on artificial intelligence*, pages 3430–3437, 2021. 2
- [55] Yifan Zhang, Qingyong Hu, Guoquan Xu, Yanxin Ma, Jianwei Wan, and Yulan Guo. Not all points are equal: Learning highly efficient point-based detectors for 3d lidar point clouds. In *Proceedings of the IEEE/CVF Conference on Computer Vision and Pattern Recognition*, pages 18953–18962, 2022. 6
- [56] Hengshuang Zhao, Li Jiang, Jiaya Jia, Philip H.S. Torr, and Vladlen Koltun. Point transformer. In *Proceedings of the IEEE/CVF International Conference on Computer Vision (ICCV)*, pages 16259–16268, 2021. 1, 3
- [57] Wu Zheng, Weiliang Tang, Li Jiang, and Chi-Wing Fu. Sessd: Self-ensembling single-stage object detector from point cloud. In *Proceedings of the IEEE/CVF Conference on Computer Vision and Pattern Recognition*, pages 14494–14503, 2021. 2
- [58] Chao Zhou, Yanan Zhang, Jiaxin Chen, and Di Huang. Octr: Octree-based transformer for 3d object detection. In *Proceedings of the IEEE/CVF Conference on Computer Vision and Pattern Recognition*, pages 5166–5175, 2023. 3
- [59] Yin Zhou and Oncel Tuzel. Voxelnet: End-to-end learning for point cloud based 3d object detection. In *Proceedings of the IEEE Conference on Computer Vision and Pattern Recognition*, pages 4490–4499, 2018. 1, 2
- [60] Zixiang Zhou, Xiangchen Zhao, Yu Wang, Panqu Wang, and Hassan Foroosh. Centerformer: Center-based transformer for 3d object detection. In *European Conference on Computer Vision*, pages 496–513. Springer, 2022. 6, 7